Electronic Supplementary Material (ESI) for Journal of Materials Chemistry A.

Supporting Information

Achieving Selective Photocatalytic CO_2 Reduction to CO on Bismuth Tantalum Oxyhalogen Nanoplates

Xiaoping Tao[a], Yi Wang[a], Jiangshan Qu, Yue Zhao, Rengui Li*, Can Li*

1. State Key Laboratory of Catalysis, Dalian Institute of Chemical Physics, Chinese Academy of Sciences, Dalian National Laboratory for Clean Energy, Zhongshan Road 457, Dalian, 116023, China.

2. University of Chinese Academy of Sciences, China.

Correspondence and requests for materials should be addressed to Rengui Li (email: rgli@dicp.ac.cn) or Can Li (email: canli@dicp.ac.cn).

Experimental Section:

1. Sample preparation

Bi_4TaO_8X (X=Cl, Br) was synthesized through two methods, solid state reaction and flux-treated method according to the previous literature.[1] For the solid state method, stoichiometric quantities of Bi_2O_3, BiOX (X=Cl, Br) and Ta_2O_5 were mixed, grounded and heated in an evacuated silica tube at 973 K for 14h. For the flux-treated Bi_4TaO_8X (X=Cl, Br), stoichiometric quantities of Bi_2O_3, BiOX (X=Cl, Br) and Ta_2O_5 with NaCl and KCl (molar ratio of NaCl / KCl is 1:1), acting as flux agents, was mixed and followed with heating in air at 973 K for 14h. The cooled mixture was washed with deionized water for several times and dried at 353 K for 5 h. BiOCl and BiOBr was prepared via a facial one-pot process as in previous reports.[2]

Different cocatalysts were loaded by in situ reduction using $NaBH_4$ as the reductive agent. Typically, a calculated amount of precursors aqueous solution was added to the aqueous suspension of photocatalyst powders (100 mg), followed with a drop wise adding of 3 mL $NaBH_4$ fresh aqueous solution (0.1 mg/mL). After stirring for 30 minutes, the sample was centrifuged and washed with deionized water for several times and dried at 353 K in a vacuum oven for 5 h.

The Bi_4TaO_8X (X=Cl, Br) and Bi_4TaO_8X-F (X=Cl, Br) film electrodes were prepared by electrophoretic deposition (EPD) on FTO substrate. Typically, the EPD was carried out in an acetone solution (50 mL) containing the powder sample (50 mg) and iodine (20 mg), before which the suspension was dispersed by continuous sonication for 20 min. The FTO electrode was immersed, paralleling with another FTO electrode, and the distance between these two electrodes was 5 cm. 20 V and 1 A were applied for 1 min using a potentiostat (ITECH IT6834), and then the prepared electrodes were calcined in air at 673 K for 1 h. The area of the electrode was fixed at 0.25 cm^2 by insulating cement.

2. Characterization of photocatalysts

The as-prepared samples were characterized by X-ray power diffraction (XRD) on a Rigaku D/Max-2500/PC powder diffractometer. Each sample powder was scanned using Cu-Kα radiation with an operating voltage of 40 kV. The scan rate of 5°/min was applied to record the XRD patterns in the range of 20-60° at a step size of 0.02°. UV-visible (UV-vis) diffuse reflectance spectra were recorded on a UV-vis spectrophotometer (JASCO V-550) equipped with an integrating sphere, scanning range, 200-800 nm, scanning rate, 200 nm/min. The morphologies and elemental compositions were examined by scanning electron microscopy (SEM, Quanta 200 FEG, FEI) with energy dispersive X-ray spectroscopy (EDX) and high resolution transmission electron microscopy (HRTEM, JEOL JEM-2000EX). X-ray photoelectron spectroscopy (XPS) measurements were conducted on a VG ESCALAB MK2 spectrometer with monochromatized Al-Kα excitation. Raman spectra were collected using 532 nm and 405 nm diode-pumped solid-state laser (Changchun New Industries Optoelectronics Technology Co., Ltd.) and a commercial Raman spectrometer (Invia, Renishaw plc.). The typical spectrum collection time was 5 s. The fluorescence spectra were measured with excitation laser beam at 405 nm output wavelength and 50-ps pulse width (Time-Tech Spectra, TPL200). In situ IR absorption experiment was carried out on a Nicolet 470 FT-IR spectrometer equipped with a homemade quartz cell and MCT (HgCdTe) detector. Ag-Bi_4TaO_8Br-F and Bi_4TaO_8Br were pressed into wafer and equipped in the middle of the cell. Ar and CO_2 through water were purged into the cell until reaching the saturation adsorption. A 300 W Xe lamp (Ushio-CERMAX LX300) equipped with optical fiber was chosen as the light source. The spectra was collected with a time period of 10 min.

3. Photocatalytic reactions

Photocatalytic CO_2 reduction was carried out in a homemade quartz reactor. 0.05 g photocatalyst was dispersed uniformly in a 5 mL saturated $KHCO_3$ solution. High purity CO_2 (99.999% Guangming Special Gas) was purged into the gastight reactor for 30min before the reaction. A 300 W Xe lamp (Ushio-CERMAX LX300) equipped with an optical cutoff filter (kenko, L42; $\lambda \geq 420$

nm) was used as the light source. The gas product was withdrawn with a syringe and analyzed by GC (Tianmei, 7900, 5A molecular sieve column with methane reformer and FID detector). For $^{13}CO_2$ labeling experiment, the reactor was purged by 99 % $^{13}CO_2$ through deionized water, with the other experiments conditions same.

The photocatalytic O_2 evolution reactions were carried out in a closed gas circulation and evacuation system using a 300 W Xe lamp (Ushio-CERMAX LX300). The photocatalyst (0.05 g) was dispersed in a 5 mL saturated $KHCO_3$ solution in a pyrex reaction cell and thoroughly degassed by evacuation in order to drive off the air inside. 50 mL CO_2 gas were injected into the system then and the amount of evolved O_2 was determined by an on-line gas chromatograph (Aglient GC7900C, TCD, Ar carrier).

The photocatalytic conversion of Fe^{3+} on Bi_4TaO_8Br and Bi_4TaO_8Br-F were carried out in an open system using a 300 W Xe lamp (Ushio-CERMAX LX300) equipped with an optical cutoff filter (kenko, L42; $\lambda \geq 420$ nm) as the light source. The photocatalyst (0.1 g) was dispersed in an aqueous 100 mL $Fe(NO_3)_3$ solution (5.0 mM) with and without methanol (10 vol%). Quantitative analysis of Fe^{2+} is conducted by a phenanthroline method. The solution after reaction was diluted that the concentration of Fe^{2+} is less than 1.0 mM. Then 1.0 mL diluted solution was mixed with 4.0 mL 0.2 M NaAc-HAc buffer solution (pH=4.0) and 3.0 mL 0.1 wt% 1, 10-phenanthroline solution (50 vol% ethanol solution). The UV-Vis absorption spectrum was measured. Then the concentration of Fe^{2+} was estimated based on the absorbance at 510 nm using a calibration curve.

4. Photoelectrocatalytic and electrochemical measurements

The photoelectrochemical performances of the Bi_4TaO_8X (X=Cl, Br) and Bi_4TaO_8X-F (X=Cl, Br) film electrodes were measured in a three-electrodes setup, where Pt electrode and saturated mercury electrode (SCE) were employed as counter and reference electrode, respectively, and 0.50 M Na_2SO_4 with or without 0.10 M Na_2SO_3 solution were used as the electrolyte solution. For linear sweep voltammetry, the potential was swept at a scanning rate of 10 mV/s. A shutter was used to record both the dark and photocurrent during a single scan. A 300 W Xe lamp (Ushio-CERMAX LX300) equipped with an optical cutoff filter (kenko, L42; □ ≥ 420 nm) was used as the light source. The charge separation efficiencies of Bi_4TaO_8Br and Bi_4TaO_8Br-F were tested by photoelectrocatalytic measurement with or without Na_2SO_3. Given that η_{inj} of the photoanode in a hole scavenger approaches 100%, the η_{sep} and η_{inj} can be estimated by $\eta_{inj} = j_{water}/j_{sulfite}$ and $\eta_{sep} = j_{sulfite}/j_{abs}$, respectively, where j_{abs} is the theoretical maximum photocurrent density determined by the light absorption as shown in Fig. S4. In order to calculate J_{max} (maximum photocurrent density) of Bi_4TaO_8Br with a band gap energy of 2.6 eV obtained from Tauc plot, the solar spectral irradiance at AM 1.5G (radiation energy ($W \cdot m^{-2} \cdot nm^{-1}$) *vs.* wavelength (nm)) was converted to the solar energy spectrum in terms of number of photons ($s^{-1} \cdot m^{-2} \cdot nm^{-1}$) *vs.* wavelength (nm). Then, the number of photons above the band gap energy of the Bi_4TaO_8Br (E_g = 2.6 eV) was calculated using a trapezoidal integration (in 10 nm increments) of the spectrum and was converted to the current density ($mA \cdot cm^{-2}$). In order to calculate J_{abs} (photocurrent assuming 100% APCE), the light harvesting efficiency (LHE) at each wavelength was multiplied during each step of the trapezoidal integration. Using these calculations, J_{max} = 4.74 mA/cm^2 and J_{abs} = 3.87 mA/cm^2 were obtained.

Electrochemical impedance spectroscopy (EIS) was carried out at the potential of 1.60 V vs. RHE, with an AC potential frequency range from 0.1 Hz to 100 kHz on a PARSTAT 2273 workstation (Princeton Applied Research) at room temperature under the irradiation of a 300 W Xe lamp (Ushio-CERMAX LX300) equipped with an optical cutoff filter (kenko, L42; λ ≥ 420 nm).

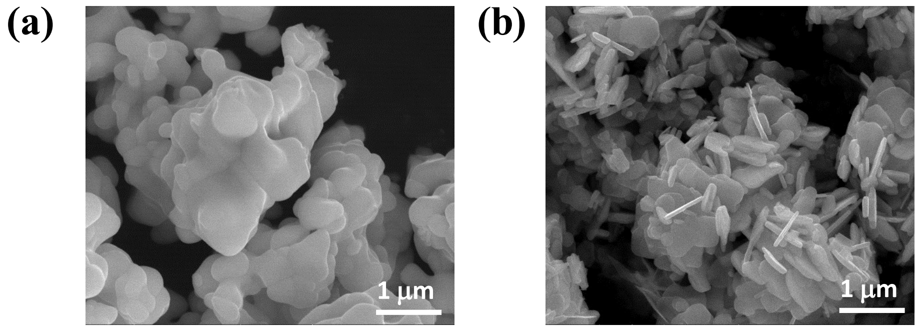

Figure S1. SEM images of Bi_4TaO_8Br (a) and Bi_4TaO_8Br-F (b).

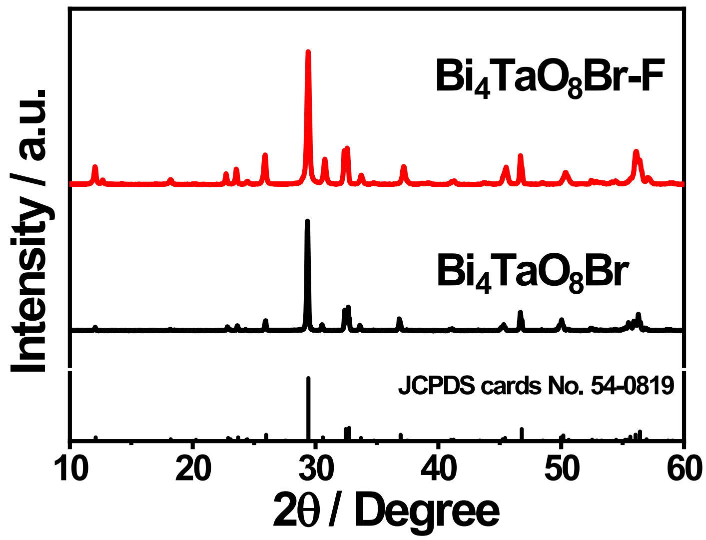

Figure S2. XRD patterns of Bi_4TaO_8Br and Bi_4TaO_8Br-F.

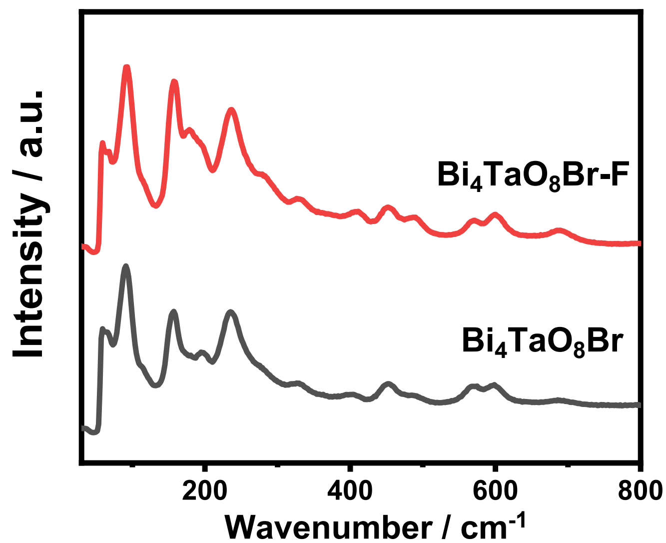

Figure S3. Raman spectra of Bi_4TaO_8Br and Bi_4TaO_8Br-F.

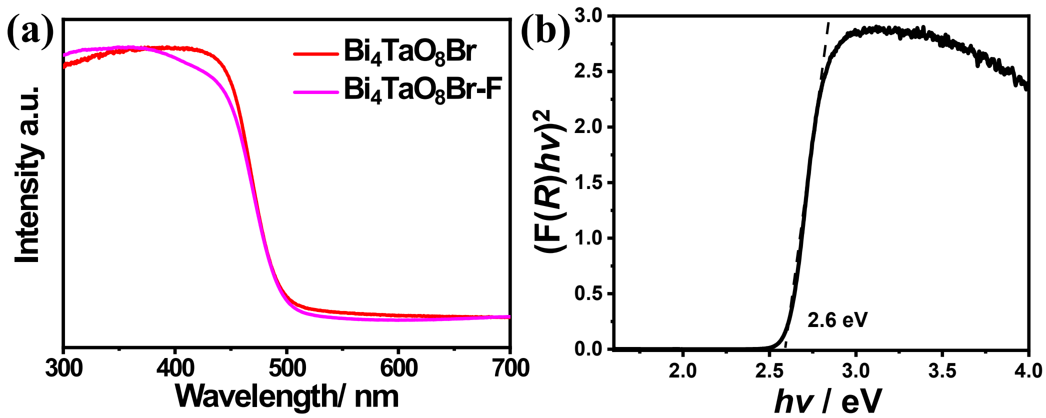

Figure S4. (a) UV-visible absorption spectra of Bi_4TaO_8Br and Bi_4TaO_8Br-F. (b) Tauc plot of Bi_4TaO_8Br.

Figure S5. Fitting results of EIS measurements of Bi_4TaO_8Br and Bi_4TaO_8Br-F.

	R_s	R_{sc}	R_{ct}
Bi_4TaO_8Br	7.9	38705	315550
Bi_4TaO_8Br-F	7.6	16293	137820

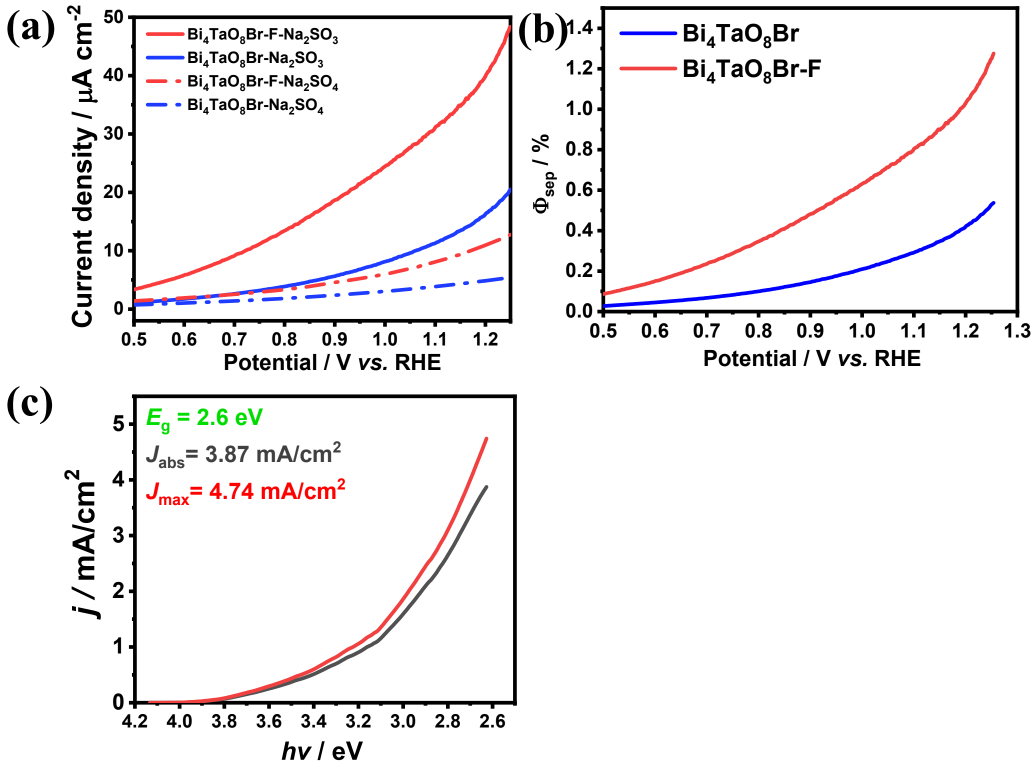

Figure S6. (a) Photoelectrocatalytic current density of Bi_4TaO_8Br and Bi_4TaO_8Br-F in the presence and absence of Na_2SO_3. (b) Φ_{sp} calculated from the J-V plots for Bi_4TaO_8Br and Bi_4TaO_8Br-F. A 0.50 M Na_2SO_4 solution containing 0.10 M Na_2SO_3 was used as the electrolyte. (c) J_{abs} and J_{max} of Bi_4TaO_8Br along the band gap.

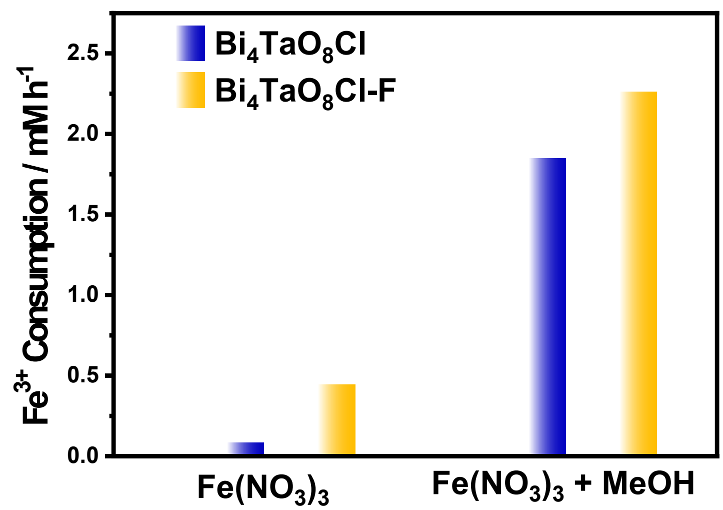

Figure S7. Photocatalytic reaction on Bi_4TaO_8Cl and Bi_4TaO_8Cl-F in the presence of $Fe(NO_3)_3$ and CH_3OH.

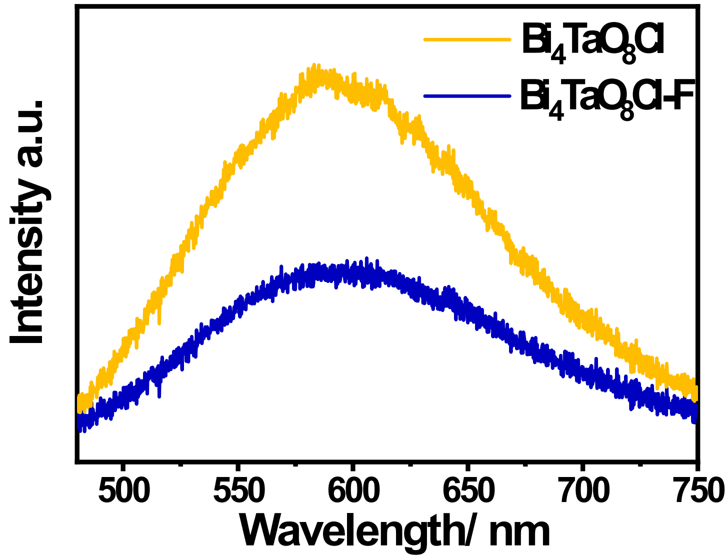

Figure S8. Steady photoluminescence (PL) spectra of Bi_4TaO_8Cl and Bi_4TaO_8Cl-F under room temperature.

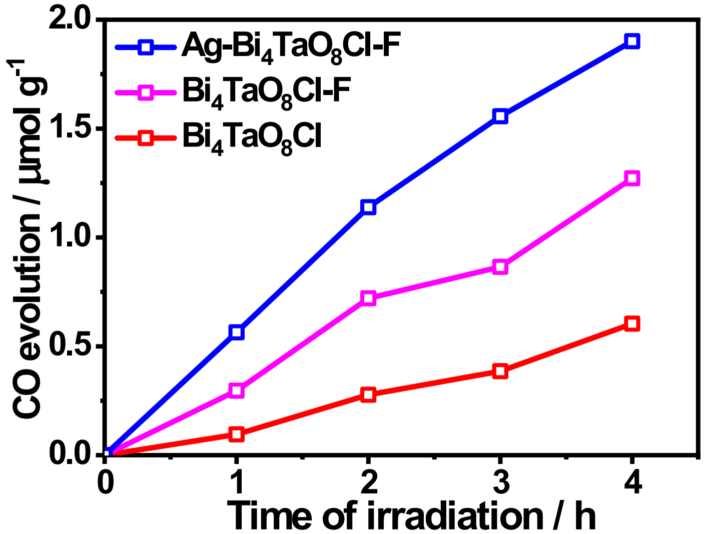

Figure S9. Time courses of photocatalytic CO_2 reduction on Bi_4TaO_8Cl, Bi_4TaO_8Cl-F and Ag loaded Bi_4TaO_8Cl-F in the saturated $KHCO_3$ solution under visible light irradiation.

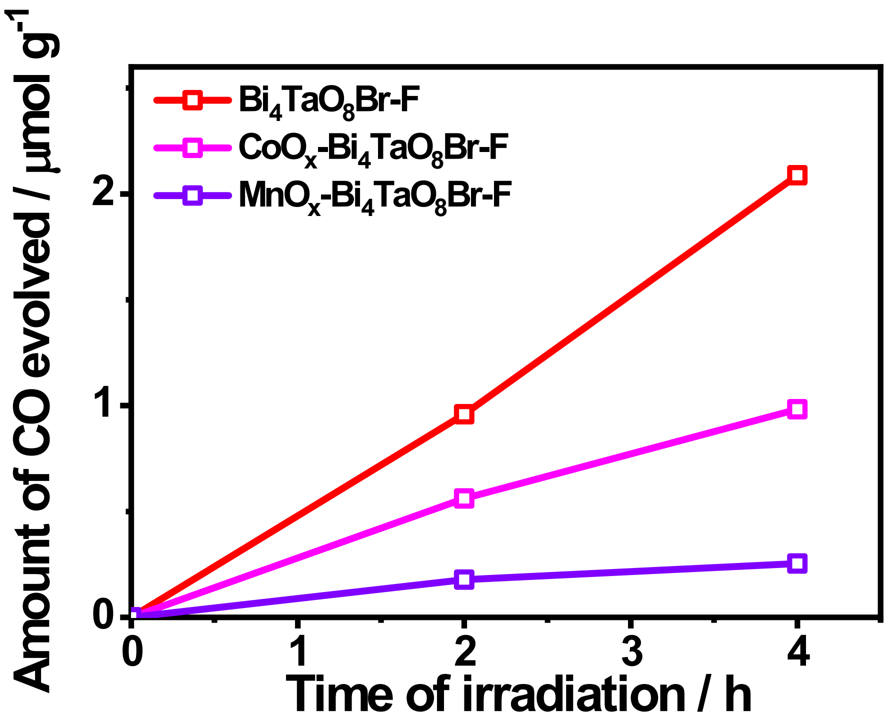

Figure S10. Time course of photocatalytic CO_2 reduction on Bi_4TaO_8Br-F loaded with CoO_x and MnO_x.

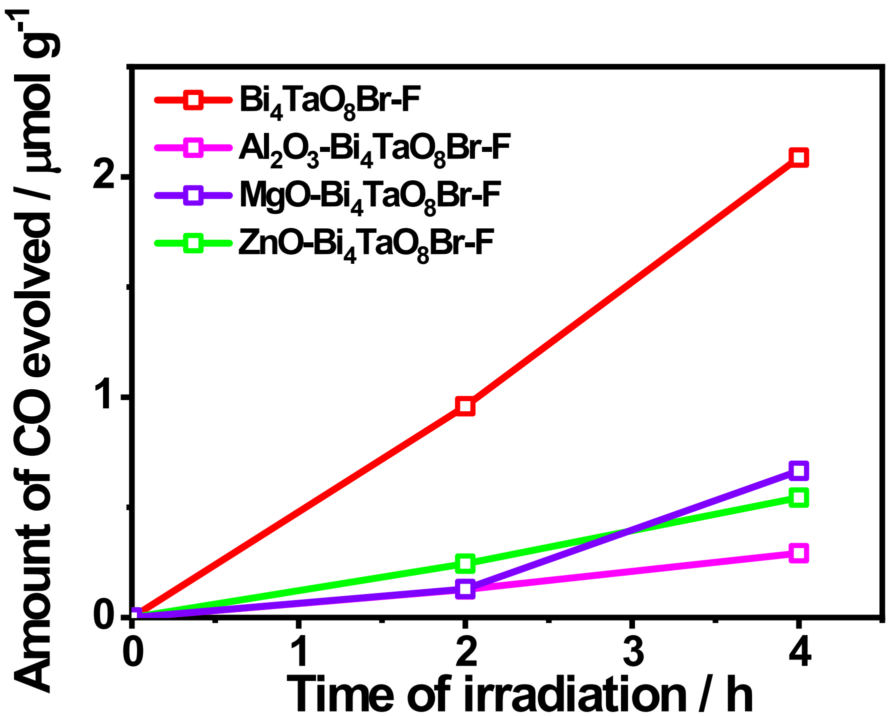

Figure S11. Time course of photocatalytic CO_2 reduction on Bi_4TaO_8Br-F loaded with Al_2O_3, MgO, and ZnO.

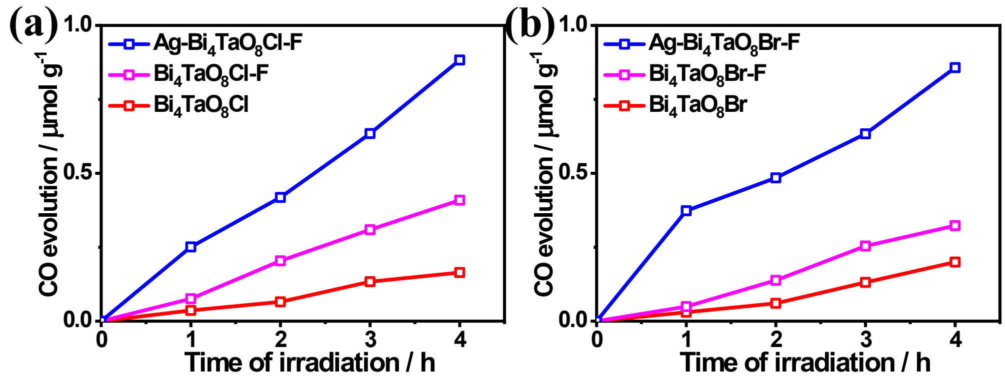

Figure S12. Time courses of photocatalytic CO_2 reduction on Bi_4TaO_8X, Bi_4TaO_8X-F and Ag loaded Bi_4TaO_8X-F (X=Cl, Br) under visible light irradiation.

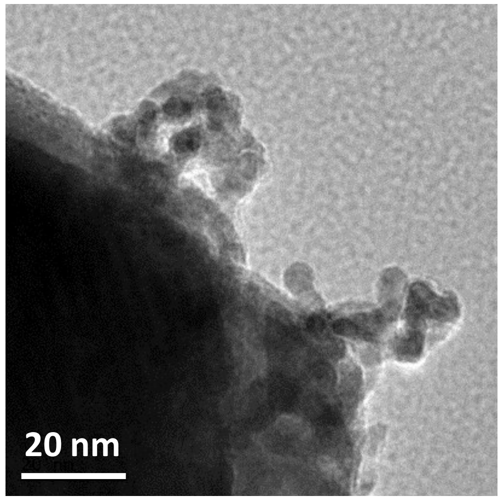

Figure S13. TEM image of Ag nanoparticles loaded on Bi_4TaO_8Br-F.

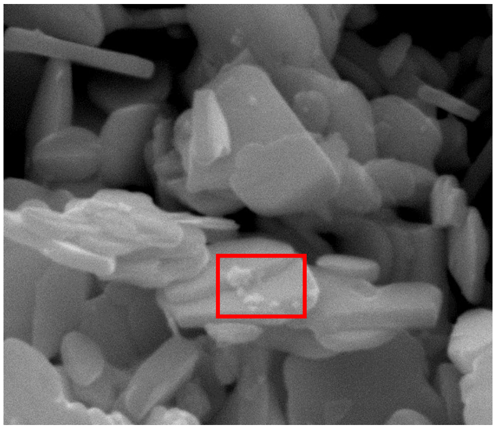 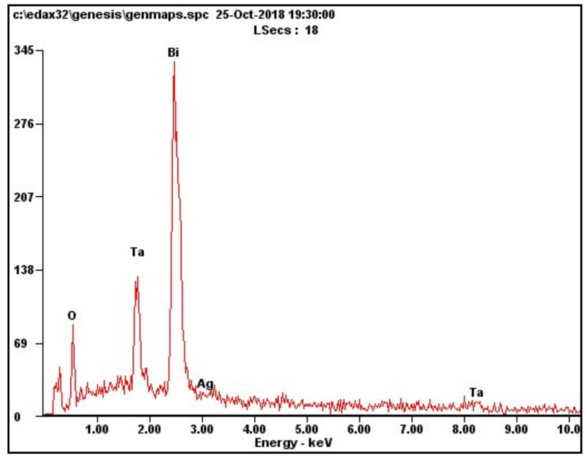

Element	Wt%	At%
OK	22.78	75.45
AgL	03.58	01.76
TaL	26.10	07.64
BiL	39.98	10.14
BrK	07.57	05.02

Figure S14. SEM image and corresponding EDX of Ag nanoparticles on Bi_4TaO_8Br-F.

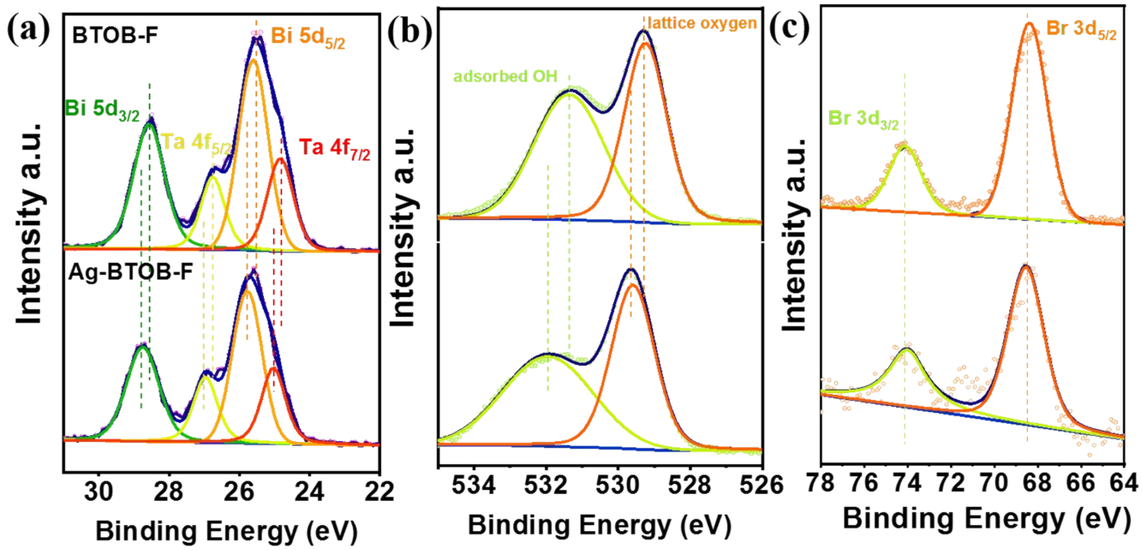

Figure S15. XPS of Bi_4TaO_8Br and Bi_4TaO_8Br-F. (a) Bi 5d and Ta 4f, (b) O 1s, (c) Br 3d.

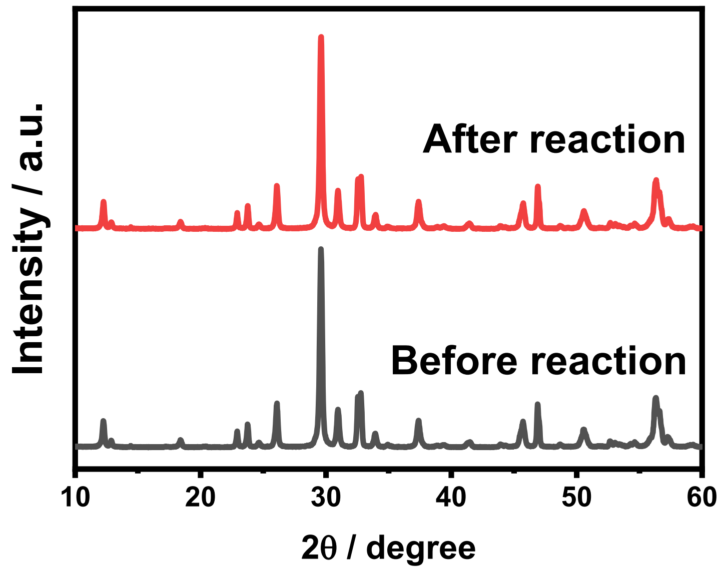

Figure S16. XRD patterns of Ag-Bi_4TaO_8Br-F before and after cycling reaction.

(a) (b)

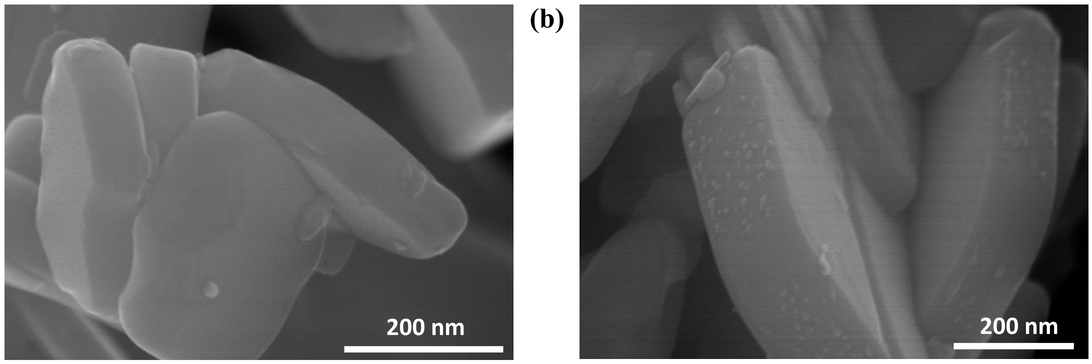

Figure S17. SEM of Ag-Bi_4TaO_8Br-F before and after cycling reaction.

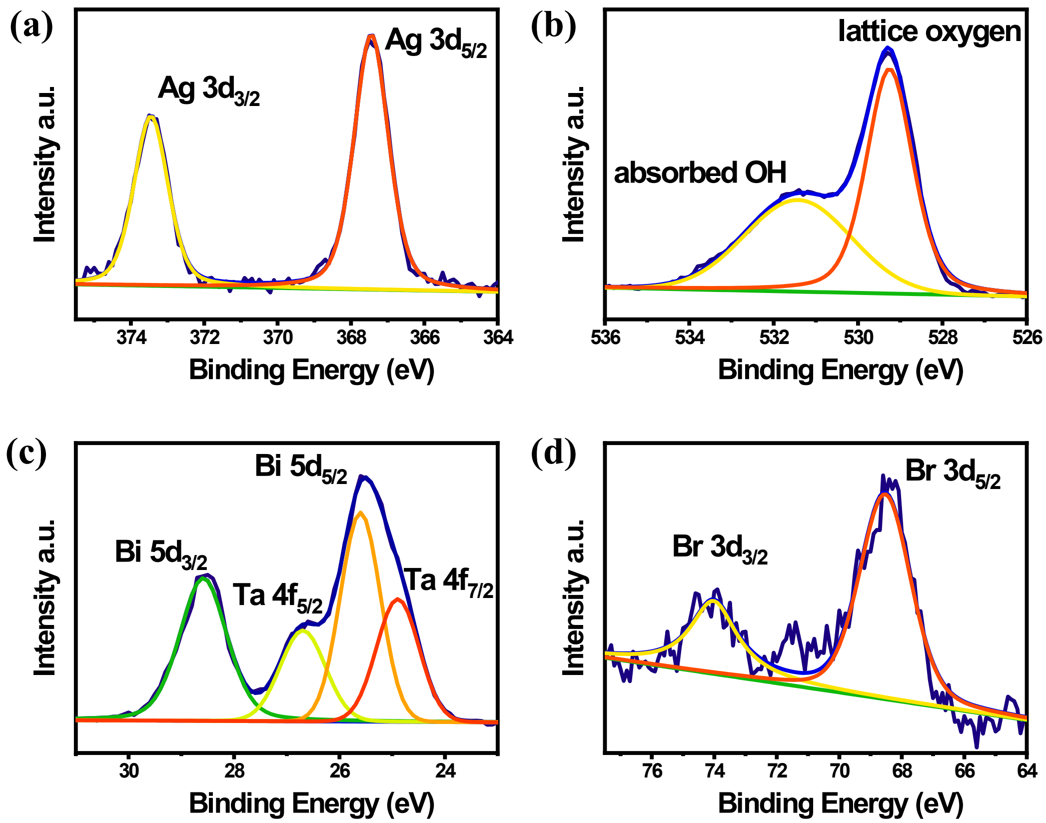

Figure S18. XPS of Ag-Bi_4TaO_8Br-F after cycling reaction.

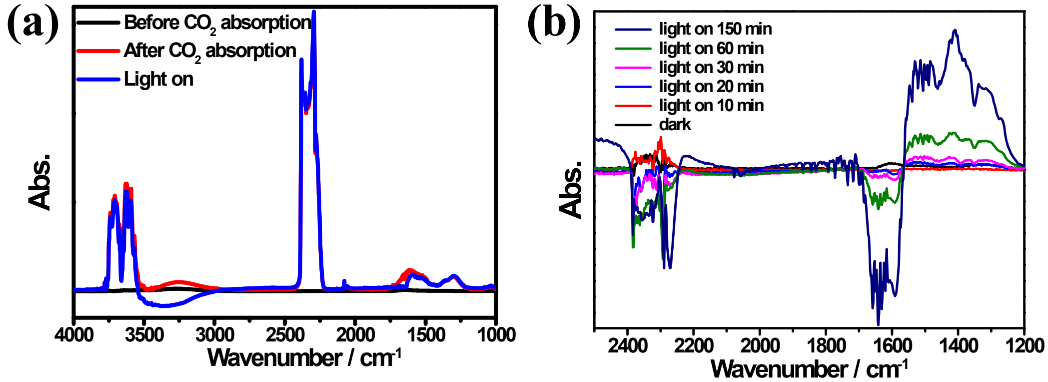

Figure S19. In situ FTIR of photocatalytic CO_2 reduction on Bi_4TaO_8Br-F before and after CO_2 absorption in dark and after irradiation for different times.

References.

1. X. Tao, Y. Zhao, L. Mu, S. Wang, R. Li and C. Li, *Advanced Energy Materials*, 2018, **8**, 1701392.
2. X. Zhang, Z. Ai, F. Jia and L. Zhang, *The Journal of Physical Chemistry C*, 2008, **112**, 747.